VNUHCM Journal of Engineering and Technology 2026, 9(2):2912-2923

Open Access Full Text Article

Research Article

Analytical approach for determining shear strength and failure modes of DE-FRP-retrofitted RC beams

Bui Van Hong Linh[1,2,*], Nguyen Thai Binh[1,2,*]

ABSTRACT

Fiber-reinforced polymer (FRP) composites have been widely used to enhance and rehabilitate reinforced concrete (RC) members subjected to shear, flexural, and axial actions due to their high strength-to-weight ratio and corrosion resistance. Among the available strengthening techniques, the embedded through-section (ETS), also referred to as the deep embedment (DE) method, has recently emerged as a highly effective solution for shear strengthening of RC beams. Experimental studies have demonstrated that ETS-strengthened beams can achieve substantially greater shear enhancement than conventional externally bonded (EB) and near-surface mounted (NSM) systems, in which FRP composites are attached to or embedded near the concrete surface. The superior performance of the ETS technique is mainly attributed to its improved anchorage and more efficient interaction with the internal shear resisting mechanisms of RC beams. This paper presents an analytical approach to evaluate the failure mechanism and shear strength of RC beams retrofitted with ETS-FRP bars. First, the shear tension-controlled capacity model previously developed by the authors is enhanced by incorporating the interaction among the shear resistances of concrete, ordinary transverse steels, and ETS-FRP bars through the effective transverse strain of the strengthening system. Three formulations for estimating the effective transverse strain of the FRP strengthening are examined. The previously developed formulations for shear compression-controlled capacity are then integrated with the enhanced model to evaluate shear behavior through variations in the major shear crack angle and the resulting shear strength. Experimental and numerical data on ETS-FRP-retrofitted beams from past works are utilized to corroborate the enhanced approach. The corroboration results show good agreement, with an average tested-to-predicted shear strength ratio of approximately 0.8 and a coefficient of variation below 20%, demonstrating the reliability of the proposed method.

Key words: Embedded through-section, FRP, Reinforced concrete, Shear model, Strengthening

[1]*Faculty of Civil Engineering, Ho Chi Minh City University of Technology (HCMUT), 268 Ly Thuong Kiet Street, Dien Hong Ward, Ho Chi Minh City, Vietnam*

[2]*Vietnam National University Ho Chi Minh City, Linh Xuan Ward, Ho Chi Minh City, Vietnam*

Correspondence

Bui Van Hong Linh, Faculty of Civil Engineering, Ho Chi Minh City University of Technology (HCMUT), 268 Ly Thuong Kiet Street, Dien Hong Ward, Ho Chi Minh City, Vietnam

Vietnam National University Ho Chi Minh City, Linh Xuan Ward, Ho Chi Minh City, Vietnam

Email: bvhlinh@hcmut.edu.vn

Correspondence

Nguyen Thai Binh, Faculty of Civil Engineering, Ho Chi Minh City University of Technology (HCMUT), 268 Ly Thuong Kiet Street, Dien Hong Ward, Ho Chi Minh City, Vietnam

Vietnam National University Ho Chi Minh City, Linh Xuan Ward, Ho Chi Minh City, Vietnam

Email: tbnguyen@hcmut.edu.vn

INTRODUCTION

The fiber-reinforced polymer (FRP) composite is often applied to enhance or restore structural performance under shear, flexural, and axial actions of reinforced concrete (RC) members. These FRP composites are typically manufactured using carbon, glass, aramid, or basalt fibers. Recently, embedded through-section (ETS) method, referred to as the deep embedment (DE) method, has been developed for strengthening beams in shear, as demonstrated by several experimental works (Mofidi et al. [1], Breveglieri et al. [2], Sogut et al. [3], Dirar and Theofanous [4], Caro [5], Bui et al. [6,7], and Azevedo et al. [8]). An illustration of the ETS technique is shown in Figure 1. The ETS technique involves installing FRP rods into holes drilled through the core section of the component. Adhesive materials are then adopted to glue the FRP bars to the concrete.

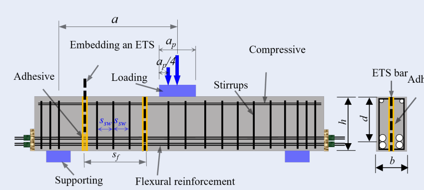

Figure 1: Illustration of ETS strengthening technique (adapted from [6,7])

The reported experimental results demonstrate that ETS-strengthened RC beams can achieve significant improvements in shear capacity compared with unstrengthened beams or beams strengthened using other techniques with near-surface mounted (NSM) approach and externally bonded (EB) approach [6]. In EB and NSM systems, FRP composites are attached to or embedded near the outer surface of the concrete member [9,10].

To determine the transverse responses of RC beams installed employing ETS-FRP rods, several analyti-

Cite this article : Linh B V H, Binh N T. **Analytical approach for determining shear strength and failure modes of DE-FRP-retrofitted RC beams**. *VNUHCM J. Eng. Technol.* 2026; 9(2):2912-2923.

History
- Received: 13-03 -2026
- Revised: 11-04-2026
- Accepted: 27-05-2026
- Published Online: 17-06-2026

DOI : https://doi.org/10.32508/vnuhcmj-et.v9i2.1579

cal approaches have been proposed in previous studies [1,6,8,11–14], including both closed-form formulations and iterative algorithms. The results reported in these studies demonstrate the capability and accuracy of the analytical models in predicting beam load–deflection response, strains in longitudinal and shear reinforcement, and concrete crack widths.

In particular, the authors' previous work (Bui et al. [13]) implemented a simplified approach to derive the shear strength and failure mechanisms of ETS-FRP-strengthened beam components by evaluating the shear-resisting forces associated with shear tension-controlled and shear compression-controlled failure modes. Validation against experimental data elucidated that the proposed approach can reasonably estimate the peak shear load of ETS-FRP-intervened specimens while correctly identifying the governing failure mode. However, in Bui et al. [13]'s model, the shear forces of concrete and internal steel stirrups are typically treated independently from that of the ETS-FRP strengthening system.

Therefore, this study attempts to incorporate the interaction among the shear-resisting components in analyzing the peak shear load of ETS-FRP-retrofitted members. To achieve this objective, the formulations proposed in Bui et al. [13] are first adopted as the basis of the analytical framework. The shear strength associated with the shear tension-controlled failure mode is then enhanced by accounting for the interaction among concrete, internal steel stirrups, and FRP DE rods through the effective transverse strain.

The enhanced model is validated using available experimental and numerical data reported in previous studies. In addition, an illustrative design example is presented to demonstrate how the proposed approach can be used to determine an optimal ETS-FRP strengthening configuration that leads to a desirable shear failure mode.

MATERIALS AND METHODS

Modified model for softened strut and tie mechanism [13]

Bui et al. [13] developed a method for determining the peak shear force of ETS-FRP-strengthened beam components on the basis of the original method of Hwang et al. [15] (Figure 2). The model was established governing on the shear tension failure with truss analogy approach ($V_{n,t}$) and shear compression failure with softened strut and tie (SST) formulations ($V_{n,c}$). Given the available studies, the present paper aims to summarize the formulations presented in Bui et al. [13]'s and Hwang et al. [15]'s works, as below:

$$V_{n,c} = K\zeta f_c' A_{str} sin\theta \qquad (01)$$

$$\zeta = 3.35/(f_c')^{0.5} \leq 0.52 \qquad (2)$$

$$A_{str} = a_s \times b_s \qquad (3a)$$

$$a_s = \sqrt{(kd)^2 + \left(\frac{a_p}{4}\right)^2} \qquad (3b)$$

$$kd = \left(\sqrt{\left(\rho_s \times \frac{E_s}{E_c}\right)^2 + 2\rho_s \times \frac{E_s}{E_c}} - \rho_s \times \frac{E_s}{E_c}\right) \times d \qquad (3c)$$

where ζ denotes the softening factor of cracked RC element; kd means to the size of the compression region (mm); θ means the inclination of the strut element (°); E_s implies the modulus of elastic of the steel (GPa); a_s denotes the strut size in depth (mm); K denotes the index involved the strut-and-tie property; b_s refers the strut size in width, taken as the web beam width b (mm); A_{str} is the effective area of a strut (mm^2); d means the effective depth of the beam section (mm); ρ_s denotes the percentage of the bottom reinforcing bars; E_c demonstrates the elastic modulus of the concrete determined by $21.5\times(f'_c/10)^{1/3}$ (GPa) [16]; a_p is the loading plate width, calculated with 100 mm.

The index represented the strut and tie action (K) for a DE-FRP-inserted specimen is derived applying the following expressions (Bui et al. [13]; Hwang and Lee [17]), as below:

$$K = K_h + K_v - 1 \qquad (4a)$$

$$K_h = 1 + (\bar{K}_h - 1)\frac{F_{yh}}{\bar{F}_h} \leq \bar{K}_h \qquad (4b)$$

$$K_v = 1 + (\bar{K}_v - 1)\frac{F_{yv}}{\bar{F}_v} \leq \bar{K}_v \qquad (4c)$$

$$F_{yh} = A_{th} f_{yh} + A_{thf} f_{fh} \qquad (4d)$$

$$F_{yv} = A_{tv} f_{yv} + A_{tvf} f_{fv} \qquad (4e)$$

$$\bar{F}_h = \gamma_h \left(\bar{K}_h \zeta f_c' A_{str}\right) cos\theta \qquad (4f)$$

$$\bar{F}_v = \gamma_v \left(\bar{K}_v \zeta f_c' A_{str}\right) sin\theta \qquad (4g)$$

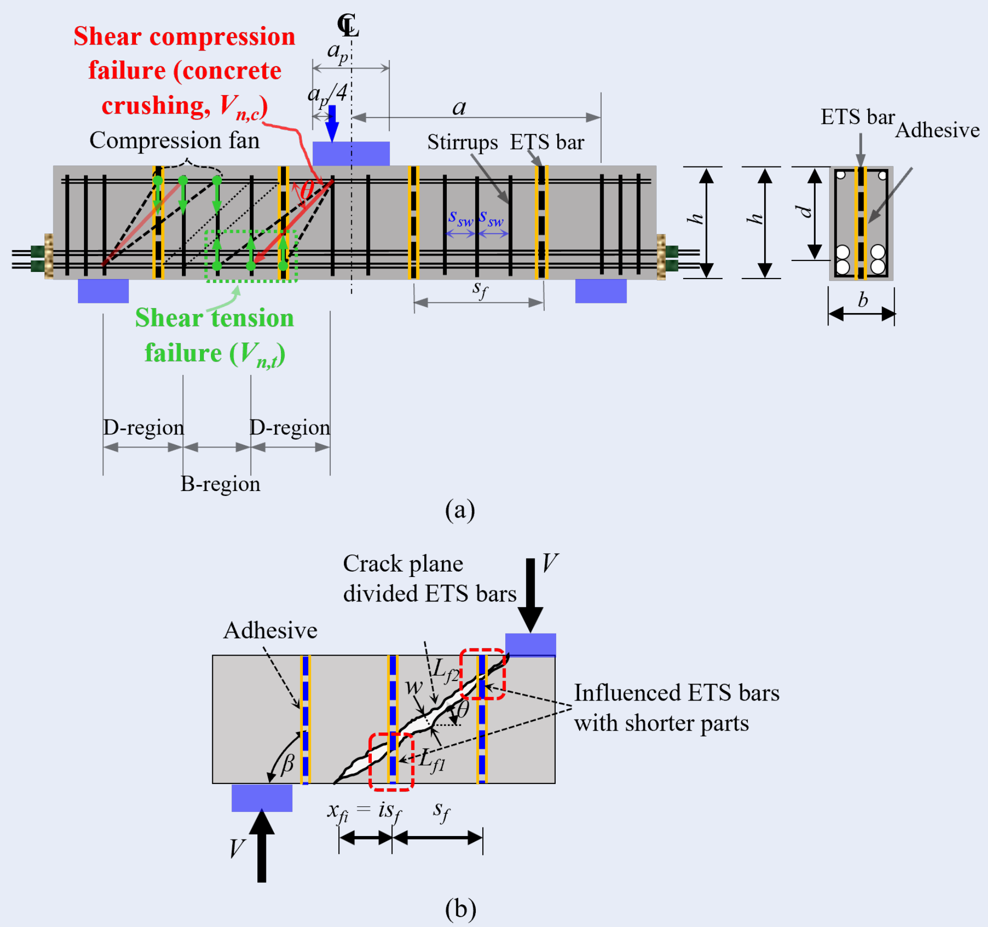

Figure 2: Shear mechanisms for an ETS-FRP-strengthened RC beam: (a) softened strut-and-tie (SST) model [13]; (b)shear resistance of ETS-FRP bars [13]

$$\bar{K}_h = \frac{1}{1 - 0.2\left(\gamma_h + \gamma_h^2\right)} \quad (4h)$$

$$\bar{K}_v = \frac{1}{1 - 0.2\left(\gamma_v + \gamma_v^2\right)} \quad (4i)$$

$$0 \leq \gamma_v = \frac{2tan\theta - 1}{3} \leq 1 \quad (4j)$$

$$0 \leq \gamma_h = \frac{2cot\theta - 1}{3} \leq 1 \quad (4K)$$

where $\overline{K_h}$ refers the horizontal tie index representing the adequacy of the horizontal stirrups; $\overline{K_v}$ is the vertical tie index representing the adequacy of the vertical stirrups; K_v and K_h mean the indices represented vertical and horizontal resisting ties, respectively; F_{yv} is the total tensile force carried by the vertical ties with the present transverse steel and FRP contributions (kN), while F_{yh} refers the force carried by the horizon-tal tie, including the contributions fromboth steel re-inforcement and FRP reinforcement(kN). A_{thf} im-plies the total area of the FRP tiesin horizontal ar-rangement (mm^2), and f_{fh} denotesthe effective ten-sile strength of the FRP horizontalties (MPa). A_{th} de-notes the area of the steelhorizontal ties (mm^2), and f_{yh} means the yieldingstrength of the horizontal steelties (MPa). A_{tvf} demonstrates the total area of the ver-tical FRP ties (mm^2), and f_{fv} is the effective strengthof the vertical FRP ties (MPa). A_{tv} implies the area of the steelvertical ties (mm^2), and f_{yv} refers the yielding strengthof the vertical reinforcing steel ties (MPa). γ_h means the amount of shear resisted by the tie in hor-izontal direction when the contribution of the verti-cal tie is neglected, whereas γ_v denotes the amountofshear resisted by the tie in vertical direction whenthe contribution of the tie in horizontal direction is not available. $\overline{F_h}$ represents the required balanced horizontal tie force (kN), while $\overline{F_v}$ illustrates the required balanced vertical tie force (kN).

Shear force for failure in shear tension ($V_{n,t}$)

The transverse force due to the shear tension failure mechanism of an ETS-FRP-strengthened beam is computed, as below:

$$V_{n,t} = V_c + k_{sf} V_{sw} + V_f \tag{5a}$$

$$V_{n,t} = bd(\sigma_{c1} cot\theta + \frac{k_{sf} A_{sw} min\left(f_{ysw},\, E_{sw}\varepsilon_{fe}\right) d}{s_{sw}} + A_f E_f \varepsilon_{fe} \left(cot\theta + cot\beta\right) \frac{h}{s_f}) \tag{5b}$$

where V_f implies the shear contribution of ETS-FRP bars (kN); f'_c denotes the maximum concrete strength under compression (MPa); V_c refers the peak shear force carried by the concrete (kN); V_{sw} means the shear resisting capacity due to the transverse steels (kN); b means the width of the specimen section (mm); A_f demonstrates the area of ETS-FRP bars (mm^2); f_{ysw} represents the stirrups yielding strength (MPa); k_{sf} = min[0.75×(1 – kd/d),1] is the coefficient considering the stirrups and ETS interaction [18]; A_{sw} is the internal stirrup area (mm^2); σ_{c1} is the concrete tensile stress (MPa); s_{sw} represents the longitudinal spacing of the ordinary steel stirrups (mm); ε_{fe} implies the effective result of the transverse strain in FRP retrofit system. For sake of convenience and simplicity, the effective transverse strain resulting in the strengthened RC member is assumed to be the same for the concrete, steel stirrups, and ETS-FRP reinforcement.

This study employs three models to calculate the transverse strain based on the effective deformation for ETS-FRP system stipulated in the JSCE [19]'s guideline, proposed using the analytical analysis of Mofidi et al. [1]'s work and Bui et al. [13]'s research, as follows:

$$\varepsilon_{fe,JSCE} = \sqrt{\left(\frac{h}{0.3}\right)^{-0.1} f'_c \frac{\rho_s E_s}{\rho_f E_f}} \times 10^{-4} \tag{6a}$$

$$\varepsilon_{fe,ACI-Mofidi} = \sqrt{\frac{8}{d_b E_f}\left(\frac{\tau_m s_m}{1+p}\right)} \leq 0.004 \tag{6b}$$

$$\varepsilon_{fe,Bui} = \frac{\pi d_f \overline{L_f} \tau_m}{E_f A_f} \leq 0.004 \tag{6c}$$

where s_m refers the slippage at corresponding to the peak bond stress (MPa); τ_m means the ultimate interfacial bond stress (MPa); p means the bond curve factor. According to the study [1], for ETS-GFRP bars, s_m applies 0.175 mm, τ_m is taken 6.0 MPa, and p is with 0.45, while for ETS-CFRP bars, s_m is with 0.176 mm, τ_m is determined at 21.3 MPa, and p is 0.125. On other hand, in work [20], the maximum bond stress (τ_m) in Eq. (7) can be calculated by:

$$\tau_m = \begin{cases} 0.07\overline{L_f}^{0.9} \; for\, \overline{L_f} \leq 90 \; (mm) \\ 9.14\sqrt{\dfrac{f_c'^{2/3} \times 0.8 \times \overline{L_f}}{E_f \rho_f + E_{sw}\rho_{sw}}} \; for\, \overline{L_f} > 90 \; (mm) \end{cases} \tag{07}$$

To determine the $\bar{L_f}$ in Eq. (12c), the FRP rods affected by the shear crack failure could be considered. As shown in Figure 2(b), when a crack forms, the ETS-FRP bars intersecting the crack surface are considered effective reinforcement. The quantity of engaged bars, the embedment length corresponding to each bar, and the mean adhered length of the FRP rods are evaluated using below expressions:

$$N_f = round\; off \left[h \frac{\cos\theta + \cos\beta}{s_f}\right] \tag{8a}$$

$$L_{fi} = \begin{cases} is_f \dfrac{\sin\theta}{\sin(\theta+\beta)} \; for\; x_{fi} < \dfrac{h}{2}(\cot\theta + \cot\beta) \\ L_f - is_f \dfrac{\sin\theta}{\sin(\theta+\beta)} \; for\; x_{fi} \geq \dfrac{h}{2}(\cot\theta + \cot\beta) \end{cases} \tag{8b}$$

$$\overline{L_f} = \frac{1}{N_f}\sum_{i=1}^{N_f} L_{fi} \tag{8c}$$

where $x_{fi} = is_f$ denotes the gap from the failure crack tip of the bar end at the beam bottom; s_f implies the spacing of ETS reinforcement (mm); N_f refers the quantity of ETS bars intersected by the major shear failure crack; θ and β denote the inclinations of the major shear crack and ETS system, respectively (°); L_{fi} means the adherence length of individual shear-engaged ETS bar (mm).

The concrete tensile strength (σ_{c1}) in Eq. (9a) is calculated using the constitutive law, as below:

$$\sigma_{cl} = \begin{cases} f_{ct} = E_c \varepsilon_1 \;\; \varepsilon_1 \leq \varepsilon_{c0} \\ max\left(\sigma_{c1,a} = f_{ct} e^{-15w}, \sigma_{c1,b} = \dfrac{f_{ct}}{1+\sqrt{2.2m\varepsilon_1}}\right) \end{cases} \tag{9a}$$

$$w = \varepsilon_1 S_{m\theta} = \varepsilon_1 \times 1/(\sin\theta/S_{ml} + \cos\theta/S_{mv}) \tag{9b}$$

Note that $S_{ml} = s_{sw}$ and $S_{mv} = d$ are simply assumed as the mean distance between shear cracks (mm); w is the size of the crack (mm); a_g is taken the average aggregate diameter (mm). Note that S_{ml} is considered

$35d/(16+a_g)$ for the specimens without internal steel stirrups. The coefficient m can be calculated as:

$$\frac{1}{m} = 4\left[\frac{\rho_{sw}}{d_{sw}}\left|\sin(90-\theta)\right| + \frac{\rho_{sl}}{d_b}\sin(0-\theta)\right] \quad (10)$$

As presented in the reference[13], the tensile strain equation of concrete is expressed as:

$$\varepsilon_1 = \varepsilon_{fe} + (0.002 + \varepsilon_{fe})cot^2(\theta)$$

The computational procedure based on the above formulations is illustrated in the flowchart shown in Figure 3. First, the beam inputs, including geometry and material properties, are defined. Then, an initial shear crack angle of $\theta = 45°$ is assumed. The calculation proceeds by gradually reducing the shear crack angle until the conditions related to shear strength are satisfied. Depending on the correlation of the values of the $V_{n,c}$, $V_{n,t}$, and θ, three failure modes of the beams, including shear-balanced, shear compression, and shear tension, can be classified as illustrated in Figure 4(a)–(c).

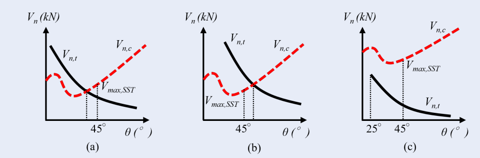

Figure 4: Failure classification: (a) shear-balanced fracture; (b) shear compression-controlled failure; (c) shear tension-controlled collapse (Source: Authors)

RESULTS AND DISCUSSION

Twenty-seven ETS-FRP-retrofitted beams experimented in the literature[1–5,7,8]. The beam configurations involved in the specimen dimensions and geometries, properties of materials, and shear capacity results served the model calculation are depicted in Table 1. Generally, the beam specimens were configured with a span containing the ETS-FRP strengthening system, while the other span was with the excessive amount of steel stirrups. The beams were intentionally failed due to the shear behavior in the ETS-strengthened span.

The validation results are reported in Table 1 and demonstrated in Figure 5. Overall, the predicted maximum shear forces show good agreement with the experimental and numerical capacities reported in the literature. The mean ratio of predicted-to-tested shear load is approximately 0.8, with a coefficient of variation (CoV) below 20%. This level of scatter indicates a reasonably consistent prediction with acceptable accuracy for analytical models of strengthened RC beams.

In general, most specimens exhibit conservative predictions, as reflected by predicted-to-tested ratios lower than unity. This tendency can be attributed to the simplified assumptions adopted in the analytical model, particularly in estimating the effective transverse strain and the interaction among concrete, steel stirrups, and ETS-FRP reinforcement, which may slightly underestimate the actual shear resistance of the strengthened members.

Among the examined formulations for effective transverse strain, the equation proposed by Bui et al.[20] provides the most accurate predictions, yielding the closest agreement with the experimental results. This improved performance may result from its ability to better represent the interfacial behavior and strain development of ETS-FRP rods adhesively embedded in concrete.

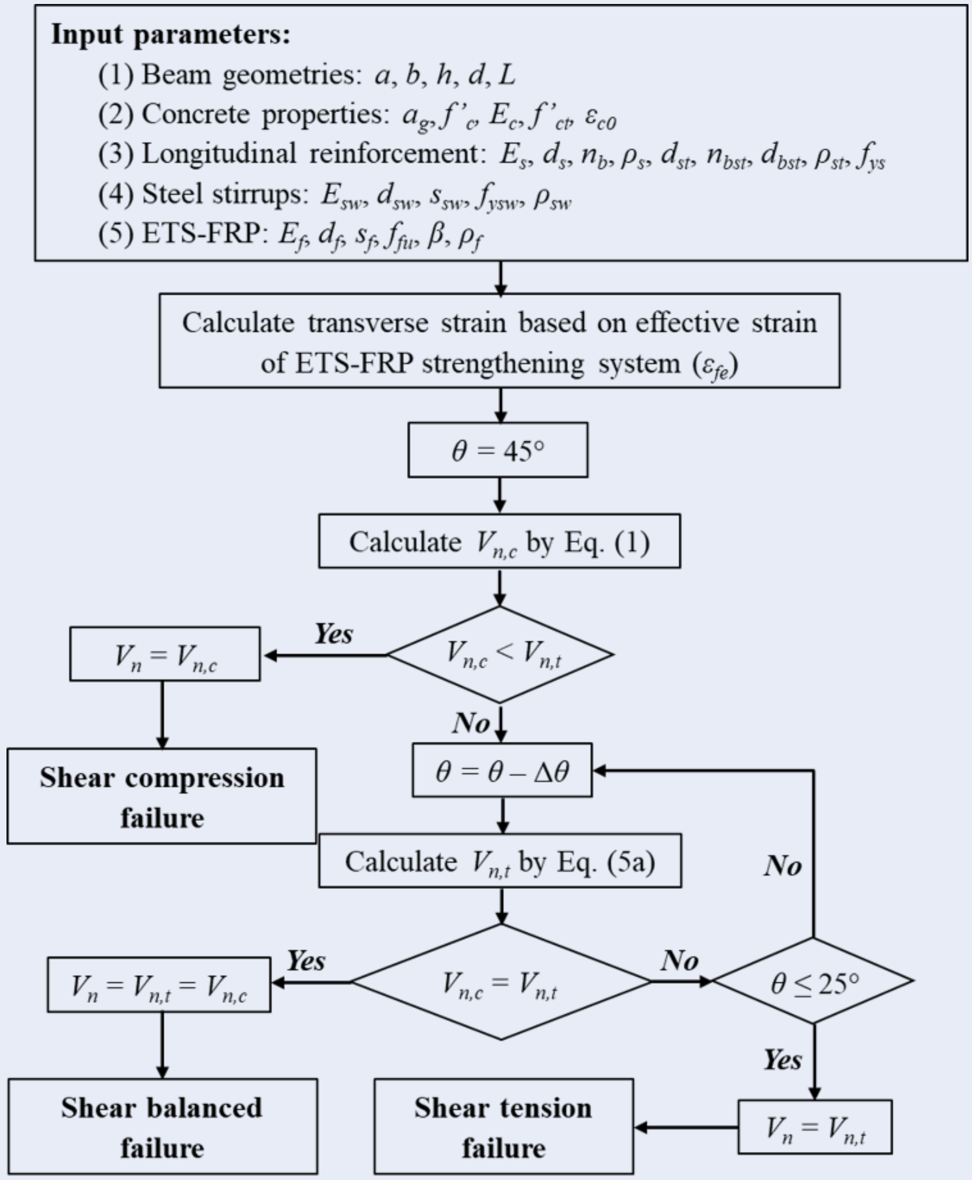

Figure 3: Calculation procedure modified from Bui et al. [13]

Table 1: Beam details[13] and verification

Studies	Beam ID	b (mm)	h (mm)	d (mm)	a (mm)	f'$_c$ (MPa)	d_s (mm)	n_b	f_{ys} (MPa)	d_{sw} (mm)	s_{sw} (mm)	f_{ysw} (MPa)	E_{sw} (GPa)
Mofidi et al.[1]	S1-9d260s	152	406	350	1050	29.6	25	4	470	8	175	540	200
	S1-12d260s	152	406	350	1050	29.6	25	4	470	8	175	540	200
	S1-9d260p	152	406	350	1050	29.6	25	4	470	8	175	540	200
Breveglieri et al.[2]	2S-C180-45	180	400	360	900	32.3	24	4	598	6	300	574	200
	4S-C180-45	180	400	360	900	32.3	24	4	598	6	180	574	200
Dirar and Theofanous[3]	C/1.9	150	650	600	1150	40	25	4	580	8	450	540	200
Caro et al.[4]	FE8-CFRP	150	650	600	1150	40	25	4	580	7	450	540	200
	FE10 (C/2.2)	150	650	600	1320	40	25	4	580	8	440	540	200
	FE11 (G/2.2)	150	650	600	1320	40	25	4	580	8	440	540	200
	FE14 (G/2.2)	150	650	600	1500	40	25	4	580	8.5	500	540	200
	FE17-CFRP	150	650	600	1150	40	25	4	580	6	450	540	200
	FE20-CFRP	150	650	600	1150	40	25	4	580	10	450	540	200
	FE26-CFRP	150	650	600	1150	40	25	4	580	8	450	540	200
	FE29-CFRP	150	650	600	1150	40	25	4	580	10	450	540	200
Sogut et al.[5]	S/2.0/G3.82	75	325	300	900	41	12	4	580	4	300	540	200
	S/2.0/G1.91	75	325	300	900	41	12	4	580	4	300	540	200
	S/2.7/G1.91	75	325	300	900	41	12	6	580	4	300	540	200
	S/2.7/C1.35	75	325	300	900	41	12	6	580	4	300	540	200
Bui et al.[7]	B2	150	300	250	900	27	25	4	390	9	300	235	200
	B3	150	300	250	1200	27	25	4	390	9	300	235	200
	B5	150	300	250	900	27	25	4	390	9	300	235	200
	B6	150	300	250	900	27	25	4	390	9	300	235	200

Continued on next page

Table 1 continued

	B7	150	300	250	900	27	25	4	390	9	300	235	200
	B8	150	300	250	900	27	25	4	390	9	300	235	200
	B9	150	300	250	900	27	25	4	390	9	300	235	200
Azevedo et al.[8]	CFRP-90	200	300	243	610	35	25	2	603	6	250	603	200
	CFRP-45	200	300	243	610	35	25	2	603	6	250	603	200

Studies	**Beam ID**	**d_f (mm)**	**s_f (mm)**	**β (°)**	**f_{fu} (MPa)**	**E_f (GPa)**	**FRP bar type**	**$V_{Exp.}$ (kN)**	**$V_{pred.}$ (Bui et al.)/$V_{Exp.}$**	**$V_{pred.}$ (Mofidi et al.)/V_{Exp}**	**$V_{pred.}$ (JSCE)/V_{Exp}**
Mofidi et al.[1]	S1-9d260s	9.5	260	90	1885	148	CFRP	260.3	0.90	1.08	0.76
	S1-12d260s	12.7	260	90	1885	148	CFRP	266.6	0.87	1.42	0.78
	S1-9d260p	9.5	260	90	2800	155	CFRP	280.7	0.82	1.03	0.71
Breveglieri et al.[2]	2S-C180-45	8	180	45	1920	160	CFRP	280.7	0.78	0.78	0.48
	4S-C180-45	8	180	45	1920	160	CFRP	370.1	0.75	0.75	0.46
Dirar and Theofanous[3]	C/1.9	12	450	90	2300	130	CFRP	426	0.80	0.80	0.57
Caro et al.[4]	FE8-CFRP	14.7	450	90	2300	130	CFRP	419.6	0.99	0.95	0.59
	FE10 (C/2.2)	12	440	90	2300	130	CFRP	322	1.08	1.08	0.77
	FE11 (G/2.2)	12	440	90	973	40	GFRP	300.4	0.72	0.71	0.71
	FE14 (G/2.2)	12	500	90	973	40	GFRP	259.5	0.81	0.80	0.80
	FE17-CFRP	12	450	90	2300	130	CFRP	390.9	0.78	0.78	0.56
	FE20-CFRP	12	450	90	2300	130	CFRP	440	0.87	0.87	0.63
	FE26-CFRP	10	450	90	2300	130	CFRP	392.5	0.73	0.73	0.60
	FE29-CFRP	10	450	90	2300	130	CFRP	427.3	0.77	0.77	0.64

Continued on next page

Table 1 continued

Sogut et al.[5]	S/2.0/G3.82	6	300	90	900	46	GFRP	68.7	0.79	0.79	0.78		
	S/2.0/G1.91	6	150	90	900	46	GFRP	78.5	0.84	0.84	0.78		
	S/2.7/G1.91	6	150	90	900	46	GFRP	90.5	0.76	0.76	0.73		
	S/2.7/C1.35	6	300	90	2300	130	CFRP	103.6	0.76	0.76	0.69		
Bui et al.[7]	B2	8	300	90	862	46	GFRP	99.2	0.72	0.74	0.77		
	B3	8	300	90	862	46	GFRP	81.5	0.88	0.90	0.94		
	B5	8	300	90	862	46	GFRP	89.1	0.88	0.82	0.86		
	B6	8	300	90	862	46	GFRP	101.9	0.70	0.72	0.75		
	B7	8	300	90	862	46	GFRP	100.2	0.71	0.73	0.76		
	B8	8	300	90	862	46	GFRP	92.1	0.77	0.79	0.83		
	B9	8	300	90	862	46	GFRP	91.5	0.78	0.80	0.84		
Azevedo et al.[8]	CFRP-90	8	250	90	2522	167	CFRP	147.85	1.03	1.09	0.79		
	CFRP-45	8	250	45	2522	167	CFRP	148.75	1.10	1.10	0.73		
								Mean	0.83	0.87	0.72		
								SD	0.11	0.17	0.12		
								CoV	0.13	0.19	0.16		

Furthermore, all analyzed beams are governed by shear tension failure, as the shear capacities calculated from the shear tension-controlled mechanism are consistently lower than those obtained from the shear compression-controlled mechanism. Consequently, the shear tension mechanism becomes the governing failure mode. This finding is consistent with experimental observations and numerical simulations reported in previous studies, where ETS-FRP-retrofitted beams often fail due to diagonal tension rather than concrete crushing in the compression strut or occurring the shear balanced failure.

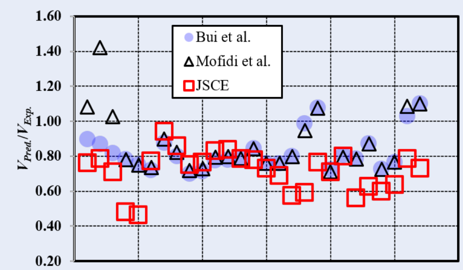

Figure 5: Validation of developed models (Source: Authors)

In design practice, achieving a shear-balanced failure mode is desirable because it allows all shear-resisting components—concrete, ETS-FRP reinforcement, and transverse steel—to be mobilized efficiently in a coordinated manner. Under this condition, neither shear-tension failure (controlled by diagonal cracking and reinforcement rupture or debonding) nor shear-compression failure (controlled by crushing of the concrete strut) occurs prematurely, resulting in a more ductile and predictable structural response. Such a balanced mechanism improves both the reliability and the effective utilization of materials.

To achieve this condition, the design should ensure compatibility between the tensile capacity of the reinforcement systems and the compressive capacity of the concrete strut. This can be accomplished by appropriately proportioning the ETS-FRP and transverse steel reinforcement, considering their spacing, orientation, and anchorage characteristics, while also accounting for the concrete strength and crack angle. An optimal design is reached when the shear contributions from concrete, ETS-FRP, and steel reinforcement are of comparable magnitude at ultimate conditions, indicating that no single mechanism governs disproportionately and that the structural capacity is fully and efficiently utilized.

As an illustrative example, consider a beam with properties similar to specimen 4S-C180-45, except for the parameters of the ETS-FRP strengthening system. An optimized strengthening configuration can be obtained with ETS-FRP bars having a modulus of elastic $E_f = 250$ GPa, an ultimate strength in tension of $f_{fu} = 2220$ MPa, a bar diameter of $d_f = 8$ mm, a spacing of $s_f = 115$ mm, and an inclination angle of $\beta = 65^\circ$. Using the proposed analytical approach, the calculated shear capacities governed by the shear tension and shear compression mechanisms become equal, yielding $V_{n,t} = V_{n,c} = 350.6$ kN.

CONCLUSIONS

This study conducts an analytical approach for determining the force in shear of beams retrofitted with DE-FRP inserting rods, considering shear tension-controlled, shear compression-controlled, and shear-balanced failure modes. In the analysis, the major shear crack angle is iteratively varied until the termination conditions are satisfied. The effective result of the strain in the ETS-FRP elements is adopted to represent the transverse strain of the RC member, implying that the strains in concrete and steel stirrups are directly related to the transverse deformation.

Validation against collected experimental and numerical data demonstrates the accuracy of the proposed approach. The mean ratio of predicted-to-tested shear load is approximately 0.8, with a coefficient of variation (CoV) below 20%. From a design perspective, achieving an optimal shear failure mode requires efficient utilization of the shear components, such as concrete, ETS-FRP strengthening reinforcement, and internal steel stirrups, so that premature failure governed by either shear tension or shear compression can be avoided.

COMPETING INTEREST

The authors declare that they have no known competing financial interests or personal relationships that could have appeared to influence the work reported in this paper.

ACKNOWLEDGMENTS

This research is funded by Vietnam National University Ho Chi Minh City (VNU-HCM) under grant number C2025-20-27.

DATA AVAILABILITY

Data sharing not applicable to this article as no datasets were generated or analyzed during the current study.

LIST OF ABBREVIATIONS

FRP — Fiber-reinforced polymer
RC — Reinforced concrete
ETS — Embedded through-section
EB — Externally bonded
NSM — Near-surface mounted
DE — Deep embedment
SST — Softened strut and tie
CoV — Coefficient of variation

AUTHOR CONTRIBUTION

Linh Van Hong Bui: Conceptualization, Data curation, Formal analysis, Funding acquisition, Investigation, Methodology, Project administration, Resources, Supervision, Validation, Visualization, Writing – original draft, Writing – review & editing.

Binh Nguyen-Thai: Conceptualization, Investigation, Methodology, Validation, Visualization, Writing – original draft, Writing – review & editing.

REFERENCES

1. Mofidi A, Chaallal O, Benmokrane B, Neale KW. Experimental tests and design model for RC beams strengthened in shear using the embedded through-section FRP method. J Compos Constr. 2012;16(5). Available from: https://doi.org/10.1061/(ASCE)CC.1943-5614.0000292.
2. Breveglieri M, Aprile A, Barros J. Embedded through section shear strengthening technique using steel and CFRP bars in RC beams of different percentage of existing stirrups. Compos Struct. 2015;126:101–113. Available from: https://doi.org/10.1016/j.compstruct.2015.02.025.
3. Sogut K, Dirar S, Theofanous M, Faramarzi A, Nayak AN. Effect of transverse and longitudinal reinforcement ratios on the behaviour of RC T-beams shear-strengthened with embedded FRP bars. Compos Struct. 2021;262:113622. Available from: https://doi.org/10.1016/j.compstruct.2021.113622.
4. Dirar S, Theofanous M. Large-scale reinforced concrete T-beams strengthened in shear with embedded GFRP bars. In: Proceedings of the 8th International Conference on Advanced Composites in Construction (ACIC 2017); 2007. p. 114–119.
5. Caro M. Shear strengthening of concrete beams with embedded FRP bars [dissertation]. . Birmingham (UK): University of Birmingham; 2018.
6. Bui L, Stitmannaithum B, Ueda T. Experimental investigation of concrete beams strengthened with embedded through-section steel and FRP bars. J Compos Constr. 2020;24(5). Available from: https://doi.org/10.1061/(ASCE)CC.1943-5614.0001055.
7. Bui L, Klippathum C, Prasertsri T, Jongvivatsakul P, Stitmannaithum B. Experimental and analytical study on shear performance of embedded through-section GFRP-strengthened RC beams. J Compos Constr. 2022;26(5). Available from: https://doi.org/10.1061/(ASCE)CC.1943-5614.0001235.
8. Azevedo AS, Firmo JP, Correia JR, Almeida J. Embedded through-section (ETS) technique for shear strengthening of reinforced concrete beams: Experimental and analytical study. Eng Struct. 2025;333. Available from: https://doi.org/10.1016/j.engstruct.2025.120038.
9. Jafari A, Shahmansouri AA. Akbarzadeh Bengar H. Hybrid CFRP-GFRP sheets for flexural strengthening of continuous RC beams: Experimentation and analytical modeling. Struct Concr. 2025;26(1):972–93. Available from: https://doi.org/10.1002/suco.202400264.
10. Hakeem IY, Osama B, Li W, Wang P, Lu Y, Sobuz M. Restoration of load capacity and stiffness of continuous steel-concrete composite beams having web openings using externally applied FRP strips. Struct Concr. 2024;25(5):3505–3530. Available from: https://doi.org/10.1002/suco.202300895.
11. Breveglieri M, Aprile A, Barros J. RC beams strengthened in shear using the embedded through-section technique: Experimental results and analytical formulation. Compos Part B Eng. 2016;89:266–81. Available from: https://doi.org/10.1016/j.compositesb.2015.11.023.
12. Bui L, Nguyen TT. Flexural-shear deformation theory (FSDT) for modeling of mechanical responses of RC beams strengthened in shear with ETS-FRP bars. Eng Struct. 2023;295. Available from: https://doi.org/10.1016/j.engstruct.2023.116830.
13. Bui L, Nguyen TT, Stitmannaithum B. Evaluation of shear strength models for ETS-FRP-retrofitted beams subjected to shear-critical failure. Eng Struct. 2024;321. Available from: https://doi.org/10.1016/j.engstruct.2024.118954.
14. Bui L, Sekiya H. Consistency of bond-slip models for analyzing ETS-FRP bar-concrete bond interface and shear contribution of ETS-FRP strengthening system. J Compos Constr. 2024;28(4). Available from: https://doi.org/10.1061/JCCOF2.CCENG-4472.
15. Hwang SJ, Yang YH, Li YA. Maximum shear strength of reinforced concrete beams. ACI Struct J. 2022;119(2). Available from: https://doi.org/10.14359/51734375.
16. CEB-FIP Model Code 90. In: Comité Euro-International du Béton (CEB). Bulletin d'Information No.213/214; 1993.
17. Hwang SJ, Lee HJ. Strength prediction for discontinuity regions by softened strut-and-tie model. J Struct Eng. 2002;128(12):1519–1545. Available from: https://doi.org/10.1061/(ASCE)0733-9445(2002)128:12(1519).
18. Spinella N. Modeling of shear behavior of reinforced concrete beams strengthened with FRP. Compos Struct. 2019;215:351–64. Available from: https://doi.org/10.1016/j.compstruct.2019.02.073.
19. Japan Society of Civil Engineers (JSCE). Recommendations for design and construction of concrete structures using continuous fiber reinforcing materials. Vol. C. ; 2007.
20. Bui L, Klippathum C, Kongmalai N, Jongvivatsakul P, Ngo DT, Stitmannaithum B. Analytical and numerical investigation of embedded through-section GFRP-strengthened RC beams with a developed bonding-based model. Eng Fract Mech. 2022;271:108595. Available from: https://doi.org/10.1016/j.engfracmech.2022.108595.

VNUHCM Journal of Engineering and Technology 2026, 9(2):2912-2923

Open Access Full Text Article

Bài nghiên cứu

Phương pháp phân tích đánh giá khả năng chịu cắt và cơ chế phá hoại của dầm bê tông cốt thép được gia cường bằng hệ thanh DE-FRP

Bùi Văn Hồng Lĩnh[1,2,*], Nguyễn Thái Bình[1,2,*]

Use your smartphone to scan this QR code and download this article

[1]*Khoa Kỹ thuật Xây dựng, Trường Đại học Bách khoa, 268 Lý Thường Kiệt, Phường Diên Hồng, Thành phố Hồ Chí Minh, Việt Nam*

[2]*Đại học Quốc gia Thành phố Hồ Chí Minh, Phường Linh Xuân, Thành phố Hồ Chí Minh, Việt Nam*

Liên hệ

Bùi Văn Hồng Lĩnh, Khoa Kỹ thuật Xây dựng, Trường Đại học Bách khoa, 268 Lý Thường Kiệt, Phường Diên Hồng, Thành phố Hồ Chí Minh, Việt Nam

Đại học Quốc gia Thành phố Hồ Chí Minh, Phường Linh Xuân, Thành phố Hồ Chí Minh, Việt Nam

Email: bvhlinh@hcmut.edu.vn

Liên hệ

Nguyễn Thái Bình, Khoa Kỹ thuật Xây dựng, Trường Đại học Bách khoa, 268 Lý Thường Kiệt, Phường Diên Hồng, Thành phố Hồ Chí Minh, Việt Nam

Đại học Quốc gia Thành phố Hồ Chí Minh, Phường Linh Xuân, Thành phố Hồ Chí Minh, Việt Nam

Email: tbnguyen@hcmut.edu.vn

Lịch sử

- Ngày nhận: 13-03 -2026
- Ngày sửa đổi: 11-04-2026
- Ngày chấp nhận: 27-05-2026
- Ngày đăng: 17-06-2026

DOI : https://doi.org/10.32508/vnuhcmj-et.v9i2.1579

TÓM TẮT

Vật liệu composite polymer cốt sợi (FRP) được sử dụng rộng rãi để tăng cường và phục hồi khả năng chịu cắt, uốn và nén của cấu kiện bê tông cốt thép (BTCT) nhờ cường độ cao và khả năng chống ăn mòn tốt. Trong các kỹ thuật gia cường hiện nay, phương pháp nhúng xuyên qua tiết diện (embedded through-section – ETS), còn gọi là nhúng sâu (deep embedment – DE), được xem là giải pháp hiệu quả cho gia cường chịu cắt dầm BTCT. Các nghiên cứu thực nghiệm cho thấy dầm gia cường ETS có khả năng tăng cường chịu cắt vượt trội so với các phương pháp dán ngoài (externally bonded – EB) và gắn gần bề mặt (near-surface mounted – NSM), trong đó FRP được dán hoặc chôn gần bề mặt bê tông. Hiệu quả của ETS chủ yếu đến từ khả năng neo tốt và sự tương tác hiệu quả với cơ chế kháng cắt bên trong dầm. Bài báo trình bày một phương pháp phân tích nhằm đánh giá cơ chế phá hoại và khả năng chịu cắt của dầm BTCT gia cường bằng thanh ETS-FRP. Mô hình khả năng chịu cắt do nhóm tác giả phát triển trước đây được mở rộng bằng cách xét đến sự tương tác giữa bê tông, cốt thép đai và thanh ETS-FRP thông qua biến dạng ngang hiệu quả của hệ gia cường. Ba công thức xác định biến dạng ngang hiệu quả của FRP được khảo sát. Các công thức cho trường hợp phá hoại nén xiên cũng được tích hợp để đánh giá ứng xử chịu cắt thông qua sự thay đổi góc vết nứt cắt chính và khả năng chịu cắt tương ứng. Kết quả kiểm chứng bằng dữ liệu thực nghiệm và mô hình tính toán cho thấy sự phù hợp tốt, với tỷ số trung bình giữa kết quả thực nghiệm và dự đoán khoảng 0.8 và hệ số biến thiên nhỏ hơn 20%, khẳng định độ tin cậy của phương pháp đề xuất.

Từ khoá: Nhúng xuyên tiết diện, FRP, Bê tông cốt thép, Mô hình chịu cắt, Gia cường

Trích dẫn bài báo này: Lĩnh B V H, Bình N T. **Phương pháp phân tích đánh giá khả năng chịu cắt và cơ chế phá hoại của dầm bê tông cốt thép được gia cường bằng hệ thanh DE-FRP**. *VNUHCM J. Eng. Technol.* 2026; 9(2):2912-2923.